Structure of Alkanethiolate Monolayers on Cu(100): Self-Assembly on the Four-Fold-Symmetry Surface

H. Kondoh, N. Saito, F. Matsui, T. Yokoyama, and T. Ohta*

Department of Chemistry, Graduate School of Science, The University of Tokyo, Hongo, Tokyo 113-0033, Japan

H. Kuroda

Research Institutes for Science and Technology, Science University of Tokyo, Noda, Chiba 278-8510, Japan

Received: July 25, 2001; In Final Form: September 21, 2001

We have studied the structure and growth process of hexanethiolate self-assembled monolayers (SAMs) on Cu(100) by means of scanning tunneling microscopy (STM) and X-ray absorption fine structure (XAFS) spectroscopy. At saturated coverage, the thiolates are assembled into a c(2 × 6) structure with zigzag chains along the close-packed Cu rows. The sulfur atom of the thiolate occupies the 4-fold hollow site of the unreconstructed Cu(100) surface with a nearest-neighbor S−S distance of 3.6 Å. Such sulfur adsorption results in a large lattice mismatch between the S/Cu layer and the alkyl chain layer, since the interchain distance of the alkyl group is ca. 4.5 Å. However, it is reconciled by the internal degree of freedom for the S−C bond which bridges the two layers, as is confirmed by the geometrical optimization based on molecular force-field calculations. The SAM film formation is well-described by a two-step process; in the first step, a full-coverage monolayer is rapidly formed, which is characterized by a highly oriented but two-dimensionally *disordered* structure, followed by a much slower evolution to the c(2 × 6) structure with surface diffusion of the thiolate.

I. Introduction

Self-assembled monolayers (SAMs) have been extensively studied because of their importance for fundamental understanding of the self-assembly mechanism as well as their technological potential for various applications.[1−3] Particularly, *n*-alkanethiolate ($CH_3(CH_2)_nS$) SAMs on Au(111) are the most thoroughly studied systems because they are easy to prepare and chemically stable and have quite highly ordered structures. The S/Au interface of the alkanethiolate SAMs on Au(111) has a $(\sqrt{3} \times \sqrt{3})R30^\circ$ commensurate hexagonal lattice, though the actual adsorption site of sulfur atoms is controversial.[4−7] The alkyl-chain packing in the SAMs exhibits a c(4 × 2) superlattice of $(\sqrt{3} \times \sqrt{3})R30^\circ$ and resembles the packing found in the bulk crystalline alkanes.[8,9] Although the bulk alkanes have a quasi-hexagonal unit mesh with a smaller lattice spacing than that of the $(\sqrt{3} \times \sqrt{3})R30^\circ$ -S structure, this lattice mismatch is accommodated by tilting of the alkyl chains to reduce the alkyl−alkyl spacing. In addition to the "c(4 × 2)" monolayer, which is the saturated phase, well-ordered flat-lying phases have been found at lower coverages.[10−14]

The structures of alkanethiolate SAMs on other metal surfaces, in particular, Ag and Cu surfaces, have been also extensively studied with a number of techniques such as X-ray and He beam diffractions,[15] scanning tunneling microscopy (STM),[16−20] near-edge X-ray absorption fine structure (NEXAFS) spectroscopy,[21,22] surface-extended X-ray absorption fine structure (SEXAFS) spectroscopy,[23−29] and the X-ray standing wave field method.[30] It was revealed that alkanethiolates adsorbed on Ag(111) form SAMs with incommensurate hexagonal lattices,[15−17] which suggests that the two-dimensional molecular arrangement in the SAMs is dominated by the intralayer interaction of the hydrocarbon rather than the molecule/substrate interaction. The smaller contribution of the molecule/substrate interaction was attributed to the shallower potential corrugation of the S/Ag interface compared to that of the S/Au one.[2] While in the case of Cu(111) the alkanethiolate/Cu interaction induces a significant substrate reconstruction[23,26,30] where surface Cu atoms are laterally displaced during ejection of some part of the surface Cu atoms. Recent STM studies[19,20] reported that alkanethiolate on Cu(111) produces a pseudo-(100) Cu surface. Therefore, in the case of Cu(100), reconstruction of the Cu(100) surface by adsorbed thiolates seems to be unfavorable. In fact, SEXAFS studies[24,27] showed that alkanethiolates on Cu(100) are located at 4-fold hollow sites without any reconstruction. Since the S/Cu interaction is believed to be stronger than the S/Au and the S/Ag interactions, molecular arrangements of the surface thiolates on the Cu surfaces should be more strongly affected by the interface structure. The 4-fold symmetry of the (100) surface conflicts with the quasi-hexagonal symmetry preferred by the alkyl−alkyl intermolecular interactions, which should cause influences on the structure and the growth process.

In this study we have investigated the structure and growth process of hexanethiol ($C_6H_{13}SH$) monolayers self-assembled on Cu(100) by using STM and C K-edge and S K-edge X-ray absorption fine structure (XAFS) spectroscopy. Since STM gives information about the two-dimensional arrangement of the surface thiolates and XAFS about the molecular local structure such as the adsorption site and orientation of the alkyl chains, the combined results of these experiments will provide comple-

* Corresponding Author. Fax: +81-3-3812-1896. E-mail:ohta@chem.s.u-tokyo.ac.jp.

10.1021/jp015517r CCC: $20.00
Published on Web 11/22/2001

mentary quasi-three-dimensional structural information of the SAMs. With the aid of geometrical optimization calculations for the alkyl chains, we propose a structural model for a saturated monolayer that is consistent with all the available experimental results. The structure and the growth process found on the Cu(100) surface are compared with those on the Au-(111) surface.

II. Experimental Section

The experiments were performed in three separate ultrahigh vacuum (UHV) chambers with base pressures less than 1×10^{-10} Torr. A Cu(100) disk was mechanically polished and electrochemically etched in a methanol solution of nitric acid. The Cu(100) surface was cleaned by repeated cycles of Ar ion sputtering and annealing. Residual carbon species were removed by the O_2 treatment (sample temperature: 350 °C, ambient O_2 pressure: 5×10^{-7} Torr). The cleanliness and ordering were confirmed by AES, XPS, XAFS, LEED, and STM. Hexanethiolate SAMs were prepared by exposing the clean Cu(100) surfaces to gaseous hexanethiol introduced via a variable leak valve at room temperature. The sample cleaning and the preparation of hexanethiolate SAMs on Cu(100) were done in the same manner in all three chambers.

The STM experiments were performed in a UHV chamber which is equipped with a bolt-on-type STM (Omicron: STM1) and facilities for low-energy electron diffraction (LEED) and Auger electron spectroscopy (AES). The coverage of the surface thiolates was monitored by the AES intensity ratio (I_{SKLL}(152 eV)/I_{CuMLL}(920 eV)). STM images were taken in the constant current mode with electrochemically etched W tips. Typical tunneling conditions used here were tunneling bias voltages ranging from 0.5 to 2.0 V and tunneling currents of around 300 pA.

C K-edge NEXAFS (280−340 eV) measurements were carried out at the plane-grating monochromator beamline BL-7A[31] of the Photon Factory (KEK-PF, Tsukuba). Spectra were taken in the partial electron yield mode using a microchannel plate (MCP) with a retarding voltage of 200 eV. The typical energy resolution was 0.5 eV around the C K-edge region. Coverages of the surface thiolates were checked by XPS intensity ratio I_{S2p}/I_{Cu3p}. The absolute coverages with respect to the surface atom density of Cu(100) (1.53×10^{15} atoms/cm^2) were determined by using the intensity ratio for a p(2×2)-S($\theta = 0.25$)/Cu(100) surface formed by exposure to H_2S at room temperature as the coverage standard. X-ray incidence angle dependence was measured to deduce molecular orientation as a function of coverage.

S K-edge NEXAFS (2460−2510 eV) and SEXAFS (2400−3000 eV) measurements were performed at the double-crystal monochromator station BL-11B[32] of the Photon Factory by the fluorescence yield method using a UHV-compatible gas-flow proportional counter with P10 gas (10% CH_4 in Ar). The energy resolution around the S K-edge region was ∼1.5 eV. The S K-edge XAFS spectra were measured with different incidence angles to obtain information on the local structure around the sulfur atom. All the S K XAFS spectra were taken at a sample temperature of 110 K.

III. Results

A. Growth Process and Structure of a Saturated Phase Observed by STM. Figure 1 shows in-situ STM observations of a Cu(100) surface during exposure to gaseous hexanethiol with a pressure of 2.5×10^{-8} Torr at room temperature. The upper part of Figure 1a is a STM image of the clean surface. A number of monatomic-height steps run along the close-packed Cu rows. Note that the lateral position of the step moves to the left-hand side with time due to thermal drift. Tip scanning proceeds from top to bottom, and the exposure started at the dotted line. Neither thiol-associated structure nor thiol-induced structural change of the substrate was observed during exposure as shown in Figure 1b,c, even though the surface coverage of thiolates reached saturation density during the scanning of the image shown in Figure 1b. The surface was not observed to change up to at least 200 L (1 L = 1×10^{-6} Torr s). The adsorption of thiolate on Cu(100) did not cause formation of any ordered structure several hours after the completion of exposure.

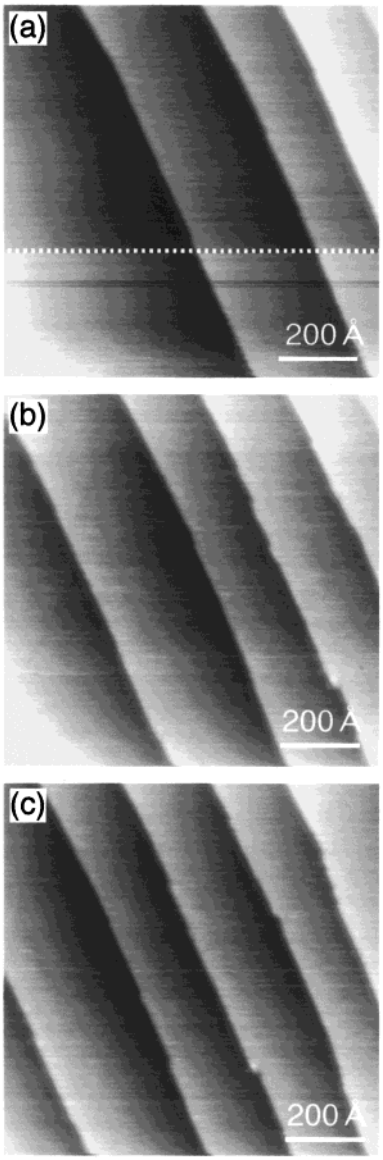

Figure 1. STM images of a Cu(100) surface taken at room temperature during exposure to gaseous hexanethiol with the pressure kept at 2.5×10^{-8} Torr. The exposure started at the dotted line during scanning of (a). Images (b) and (c) were taken 3 and 7 min later, respectively. The coverage reached a saturated monolayer while scanning the image (b). No ordered structure was observed during exposure even though the exposure was continued for more than 2 h.

Figure 2 shows STM images of Cu(100) surfaces with different thiolate coverages taken a long time (>24 h) after exposure. At low coverages, no thiol-associated feature was observed even after 24 h, as shown in Figure 2a. At 0.7 ML (here, the coverage of the saturated phase is defined as 1 ML),

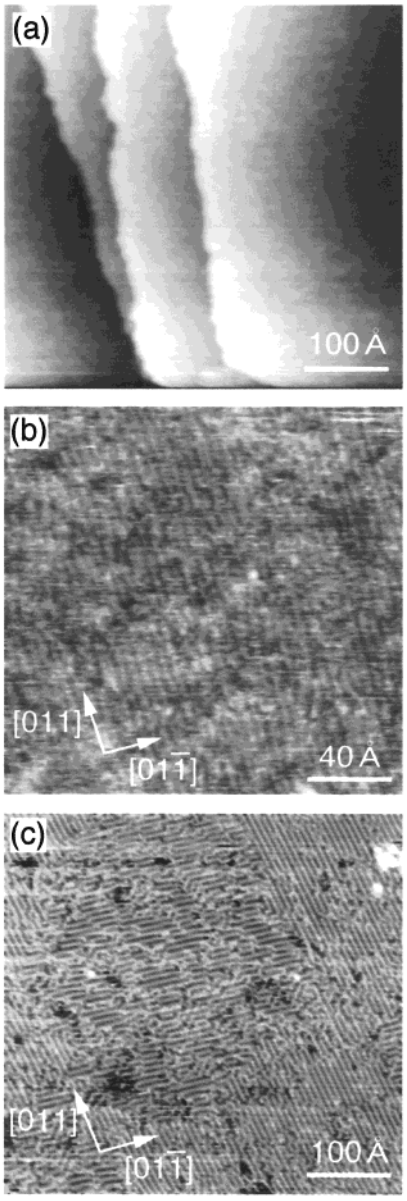

Figure 2. STM images of hexanethiol-adsorbed Cu(100) surfaces with different coverages at thermal equilibrium; (a) 0.4 ML, (b) 0.7 ML, and (c) 1.0 ML. The coverage of the saturated monolayer is defined as 1 ML here. These images were taken a prolonged time (>24 h) after the completion of exposure.

however, faint stripes appear nearly periodically. The stripes are aligned along the close-packed Cu rows ([011]and [01$\bar{1}$] directions) with an inter-stripe periodicity of approximately 5 Å. Furthermore, at 1 ML, the saturation density, the surface is covered with striped domains as shown in Figure 2c. There are two domains mutually rotated by 90°, of which stripes are aligned parallel to the [011] and [01$\bar{1}$] directions. The observed domains contain many defects and anti-phase boundaries.

Figure 3 shows a molecular image of a saturated-phase-covered Cu(100) surface. The molecular image revealed that one stripe consists of double rows of bright protrusions with a period of 5.0 ± 0.3 Å along the row, which is in accordance with the doubled distance of the nearest Cu−Cu distance (2.56 Å). Since the nearest neighbor (NN) intermolecular distance inside the double row is observed to be rather short (3.3 ± 0.3 Å), it appears to be a "dimer-row". The dimer-row spacing is 7.5 ± 0.3 Å, which is three times longer than the nearest Cu−Cu distance. Thus, the unit cell of this structure is identified as

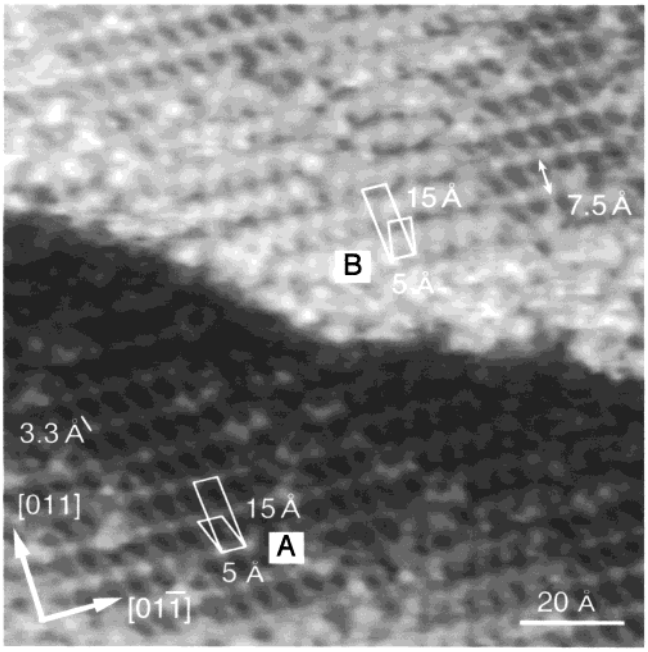

Figure 3. Molecular-resolution STM image of a hexanethiol-saturated Cu(100) surface at thermal equilibrium. The unit cell of the ordered structure is identified as commensurate c(2 × 6) as indicated in the figure. Two rotated domains with rotation angles of ±18° with respect to the [011] direction are observed as denoted by A and B.

commensurate c(2 × 6) (5 × 15 Å rectangle) as indicated in the figure. This identification is supported by LEED observations in which a clear c(2 × 6) pattern was observed as shown later. It should be noted that the distance between NN bright protrusions is found to be only 3.3 Å, which is much shorter than the intermolecular distances in alkanethiolate SAMs on metal surfaces studied so far, such as Au(111), Au(100), and Ag(111) (4.5−5.0 Å).[1−3,15−17,33] Careful observation of Figure 3 reveals that there are two domains, A and B, which are rotated clockwise and counterclockwise with respect to the substrate [011] direction by 18 ± 3°. These rotated domains might be associated with azimuthal rotation of alkyl chains and their structure will be discussed in detail later.

B. LEED and XPS Results for the Saturated Phase. LEED observations also indicated that the thiolates form an ordered structure at around the saturation coverage, as shown in Figure 4. This pattern is identified as diffraction spots from two 90°-rotated domains of a commensurate c(2 × 6) lattice. Very recently, the same diffraction pattern has been observed for ethanethiol (C_2H_5SH) and heptanethiol ($C_7H_{15}SH$) monolayers on Cu(100) by LEED and He atom scattering.[34] The c(2 × 6) LEED pattern vanished within 30−200 s due to electron-induced destruction of the surface ordering. This pattern was not seen just after exposure but became observable after more than 8 h. At lower coverages no thiolate-induced LEED pattern was observed even 24 h after exposure. To determine the coverage of the saturated phase we measured S 2p XPS spectra (not shown) from a saturated monolayer and a p(2 × 2)-S ($\theta = 0.25$) adlayer on Cu(100). From the comparison of the peak intensity, the coverage of the thiolates in the saturated phase is estimated to be 0.30 ± 0.03 with respect to the Cu atoms in the first layer.

C. Molecular Orientation Change Deduced from C K-Edge NEXAFS. Figure 5 shows C K-edge NEXAFS spectra from hexanethiolate SAMs on Cu(100) with coverages of 1 and 0.4 ML taken just after exposure. In the 1 ML spectra two prominent peaks are observed at 288 and 293 eV and are

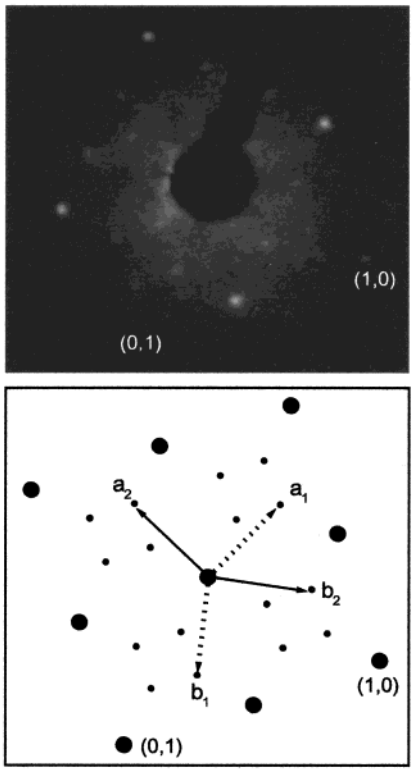

Figure 4. LEED pattern for the hexanethiol-saturated Cu(100) surface and its schematic sketch. The c(2 × 6) unit cells for two 90°-rotated domains are indicated by two pairs of arrows ((a_1, b_1) and (a_2, b_2)).

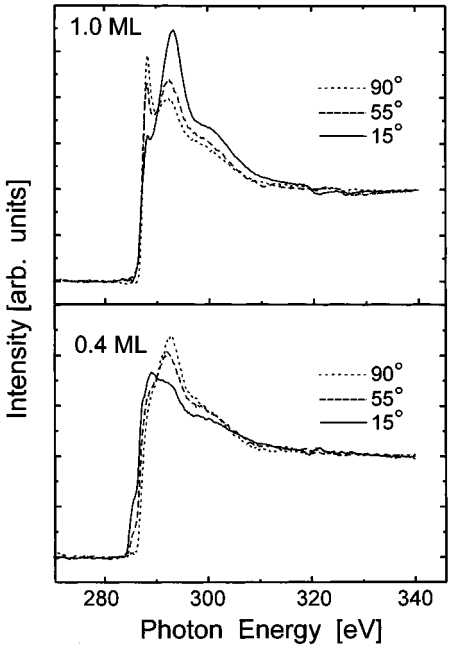

Figure 5. C K-edge NEXAFS spectra of hexanethiol-adsorbed Cu(100) surfaces with different coverages, 1.0 ML (upper) and 0.4 ML (lower). The spectra of these surfaces exhibit opposite polarization dependence.

attributed to the excitations from C 1s to a Rydberg/σ^*(C−H) state and a σ^*(C−C) state, respectively.[35,36] Since the σ^*(C−C) peak is most enhanced at the grazing incidence, the molecular axis is aligned with a standing-up configuration. On the other hand, the σ^*(C−C) peak at 0.4 ML exhibits opposite polarization dependence compared to that for 1 ML, indicating a molecular axis lying down on the surface. The lower-energy peak observed at 288 eV consists of several components with

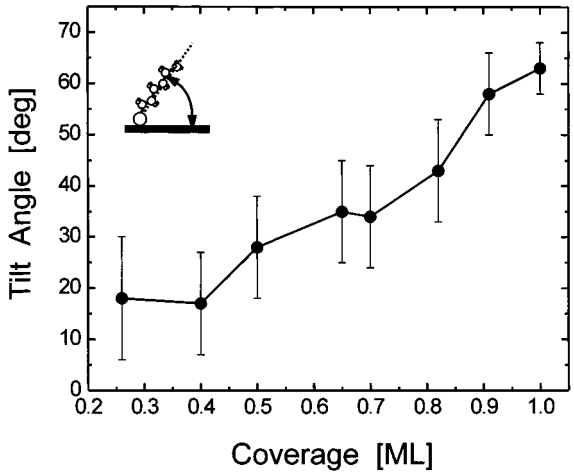

Figure 6. Change of molecular orientation of hexanethiol adsorbed on Cu(100) derived from the C K-edge NEXAFS results as a function of coverage.

transition moments lying along different directions.[37] Quantitative analysis of the polarization dependence of the σ^*(C−C) peak indicates that the orientation angle of the molecular axis for 1 and 0.4 ML is 27 ± 5° and 73 ± 10°, respectively, from the surface normal.[38] In Figure 6 the orientation angle is plotted as a function of coverage. The coverage dependence of the orientation angle indicates that the molecular axes lie almost flat at low coverages below 0.4 ML and gradually stand up with increasing coverage. The orientation angle finally reaches 27 ± 5° from the surface normal which is similar to that found in the SAMs on Au(111).[9] We did not observe noticeable change of the C K-edge NEXAFS spectra even a prolonged time after exposure.

D. Interface Structure of the Saturated Phase Determined by S K-Edge XAFS. The STM observations showed that the saturated monolayer needs a long aging time (>8 h) to form the 2D-ordered structure, though the alkyl chains were well oriented just after adsorption as indicated by C K-edge NEXAFS. To understand the time-dependent change of the structure at the S/Cu interface, we measured S K-edge NEXAFS and SEXAFS spectra for a saturated monolayer after different aging times. Figure 7 shows S K-edge NEXAFS spectra from two samples; one was quenched to 110 K immediately after adsorption and another was cooled to 110 K after aging for 36 h at room temperature. No significant change is observed after long-time aging, indicating quite a similar local geometric and electronic structure around the sulfur atom. A prominent peak at 2473.9 eV observed in the grazing-incidence spectra is attributed to the excitation to σ^*(S−C).[39] Since the σ^*(S−C) transition is most enhanced at grazing incidence, the S−C bonds are vertically oriented. The curve-fitting analysis indicated that the S−C bond angles in the quenched and the aged samples are $\theta = 15 \pm 10°$ and $19 \pm 10°$, respectively, from the surface normal. It is noted that a small feature is observed as a shoulder at the pre-edge region, whose polarization dependence is opposite to that of the σ^*(S−C) resonance. A similar peak was also observed for hexanethiolate adsorbed on Ag(100).[29] On the basis of the ab initio quantum chemical calculations for a methylthiolate adsorbed on noble metal surfaces,[40] this feature is associated with the lowest π-type unoccupied state of the thiolate, which is characterized by S 3p and C 2p of the S−C bond.

The SEXAFS oscillation functions $k^2\chi(k)$ for the two samples were obtained by means of standard analysis procedures: pre- and post-edge subtraction and normalization with the atomic

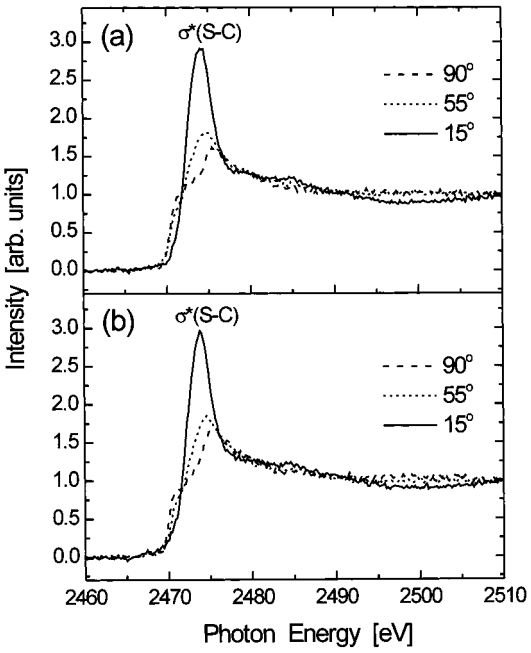

Figure 7. S K-edge NEXAFS spectra of hexanethiol-saturated Cu(100) surfaces. The spectra were taken (a) when the sample was quenched to 110 K just after exposure, and (b) after 36-h aging at room temperature. A prominent peak at 2973.9 eV is due to the excitation to σ^*(S−C). A shoulder structure at the pre-edge region exhibits polarization dependence opposite to the σ^*(S−C) resonance.

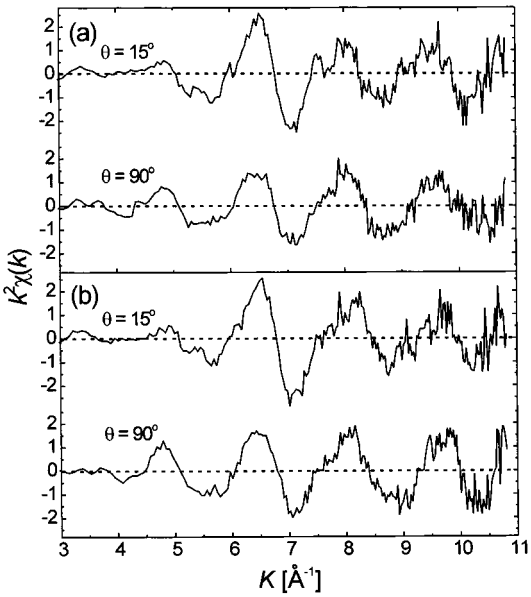

Figure 8. S K-edge SEXAFS oscillation functions $k^2\chi(k)$ obtained for hexanethiol-saturated Cu(100) surfaces. The spectra were taken (a) when the sample was quenched to 110 K just after exposure and (b) after 36-h aging at room temperature.

absorption coefficients.[41,42] The resultant $k^2\chi(k)$ functions are shown in Figure 8, and corresponding Fourier transforms ($\Delta k = 3.0\sim10.6$ Å^{-1}) are depicted in Figure 9. To determine the adsorption site we analyzed polarization dependence of the effective coordination number of the S−Cu(1) shell using $\chi(k)$ of the CH_3S/Cu(100) system[24] as the standard, where the coordination number and the S−Cu(1) distance are $N = 4$ and $R = 2.29$ Å. The results are compared with calculated values for high-symmetry sites of the unreconstructed substrate as listed in Table 1. The experimental results for the two samples are in good agreement with those for the 4-fold hollow site. The

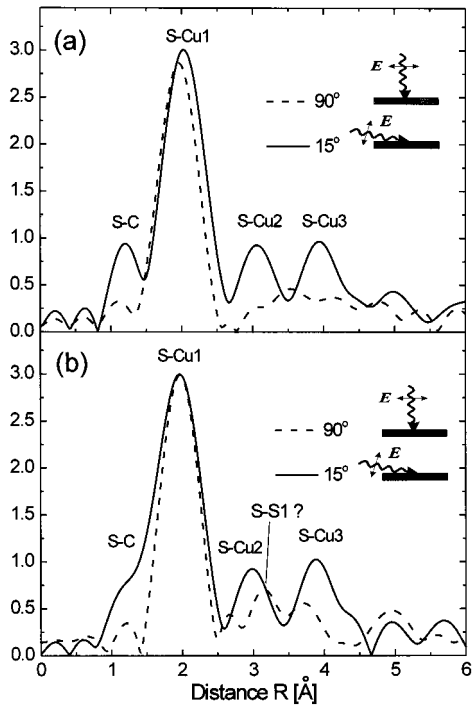

Figure 9. Fourier transforms of S K-edge SEXAFS oscillation functions $k^2\chi(k)$ (Figure 8) of the samples (a) quenched to 110 K just after exposure and (b) after 36-h aging at room temperature.

TABLE 1: Effective Coordination Numbers and Their Ratio for the S−Cu(1) Shell[a]

	N(90°)	N(15°)	N(90°)/N(15°)
	Quenched Sample		
atop	0	2.72	0
bridge	0.95	3.81	0.25
hollow	3.78	4.37	0.86
expt	3.87 ± 0.25	4.28 ± 0.25	0.90 ± 0.09
	Aged Sample		
atop	0	2.72	0
bridge	0.96	3.78	0.26
hollow	3.85	4.26	0.90
expt	3.84 ± 0.25	4.22 ± 0.25	0.91 ± 0.11

[a] The experimental results are compared with calculated values for the sulfur atom at high-symmetry sites of the unreconstructed Cu(100) substrate with a S−Cu(1) distance of 2.28 Å (quenched sample) and 2.26 Å (aged sample) that were determined by the curve fitting as described below.

TABLE 2: The Structure Parameters for the Local Structure around the Sulfur Atom Derived from S K-edge SEXAFS[a]

	quenched sample	aged sample
R(S−C) [Å]	1.82 ± 0.04 (1.819)[c]	1.85 ± 0.05 (1.819)[c]
R(S−Cu(1)) [Å]	2.28 ± 0.02	2.26 ± 0.02
ω(S−Cu(1)) [°][b]	53 ± 3 (52.6)[d]	53 ± 3 (53.2)[d]
R(S−Cu(2)) [Å]	3.20 ± 0.03 (3.20)[d]	3.16 ± 0.03 (3.16)[d]

[a] Curve fitting analyses in k space were performed after Fourier filtering of the contribution of interest; S−C (ΔR = 0.8−1.4 Å), S−Cu(1) (ΔR = 1.5−2.5 Å), and S−Cu(2) (ΔR = 2.6−3.4 Å) shells. [b] S−Cu(1) bond angle from the surface normal estimated from the effective-coordination-number ratio. [c] The S−C bond length of gaseous methanethiol. [d] Calculated values for adsorption at four-fold hollow sites of the unreconstructed and unrelaxed substrate with a S−Cu(1) distance of 2.28 Å (quenched sample) and 2.26 Å (aged sample).

structural parameters around the sulfur atom were determined as shown in Table 2. For the aged sample the S−Cu(1) distance is R(S−Cu(1)) = 2.26 ± 0.02 Å, and its bond angle is ω(S−

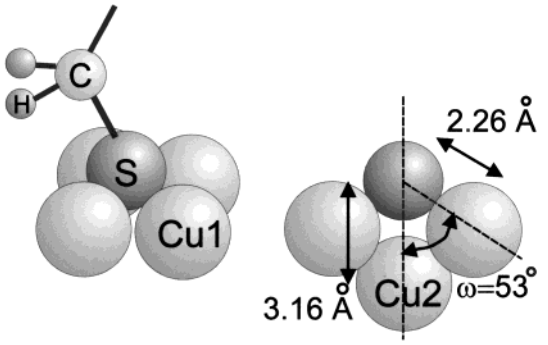

Figure 10. Schematic illustration for the local structure around the sulfur atom in the aged sample deduced from S K-step SEXAFS.

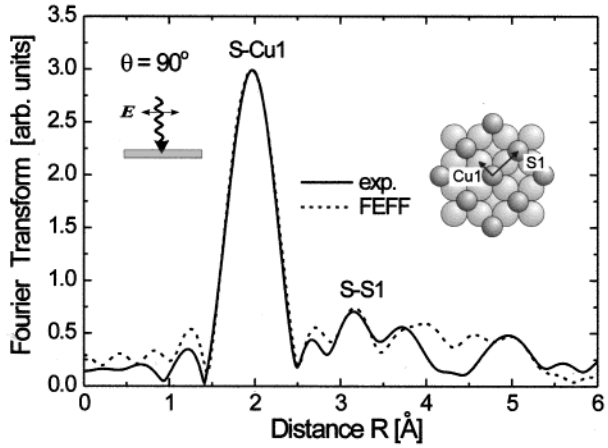

Figure 11. Fourier transform of the SEXAFS oscillation for the aged sample and a simulation curve calculated with the FEFF8 code based on a cluster model shown in the Inset. In the model, sulfur atoms occupy the 4-fold hollow sites of the unreconstructed substrate forming a c(2 × 2) lattice. Since a peak at around 3.2 Å in the calculated curve is due to S−S1 ($R = 3.62$ Å) scattering, the corresponding peak observed in the experimental curve is attributed to scattering from the nearest-neighbor sulfur atoms at the same distance as for a c(2 × 2) lattice.

Cu(1)) = 53 ± 3°. The distance to the second NN Cu atom is R(S−Cu(2))=3.16 ± 0.03 Å. The local structure around the sulfur atom for the aged sample is schematically illustrated in Figure 10. The obtained values for ω(S−Cu(1)) and R(S−Cu(2)) are in accordance with the calculated values for the unreconstructed substrate. Similar good agreement is also seen for the quenched sample. Therefore it is concluded that the sulfur atoms are situated at the hollow site without reconstruction irrespective of the aging time.

Although no drastic change is observed after 36-h aging for either the $k^2\chi(k)$ functions or Fourier transforms, we can find an appreciable difference, particularly in the normal-incidence curve of the Fourier transform. For the quenched sample, no specific peak is observed at above 3 Å, while for the aged sample, a new peak appears at 3.2 Å. One possible origin of this peak is that it comes from the NN sulfur atoms. To check this possibility, we compare the data with simulation curves calculated with the FEFF8 code[43] based on a cluster model shown in the inset of Figure 11. In this model, sulfur atoms are located at 4-fold hollow sites of the unreconstructed substrate forming a c(2 × 2) lattice. The experimental curves are well reproduced by the simulation as shown in Figure 11. The scattering from the NN sulfur atoms in the c(2 × 2) lattice certainly gives rise to a peak at 3.2 Å. The curve-fitting analysis in k space has been performed after Fourier filtering of the contribution of the 3.2 Å peak ($\Delta R = 2.9-3.4$ Å) using $\chi(k)$ for the S−S(1) shell calculated by FEFF8 as the standard. The

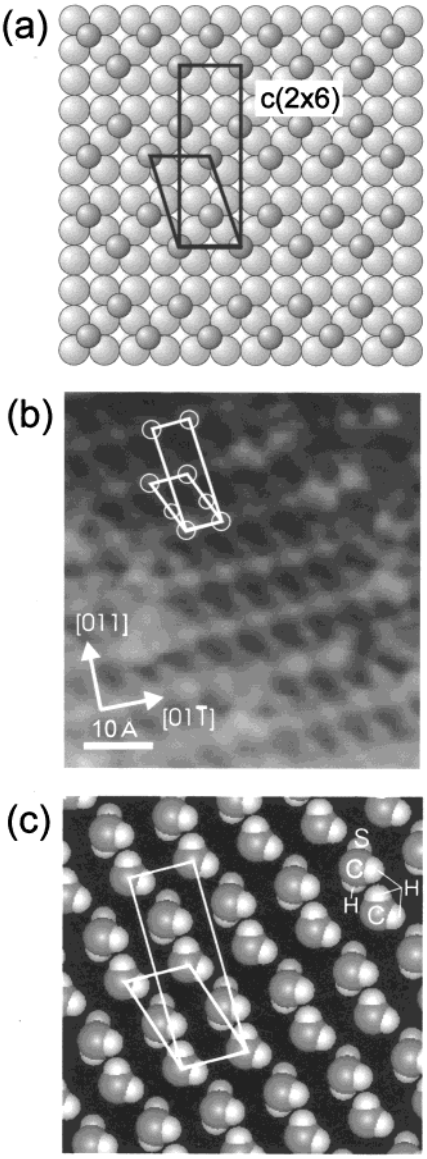

Figure 12. (a) Structural model for arrangement of the sulfur atoms of the thiolates on Cu(100) with saturated coverage deduced from SEXAFS using a unit cell (c(2 × 6)) and molecular density ($\theta = 0.30 \pm 0.03$). The molecular density of this model is $\theta = 0.33$. (b) Molecular image of a saturated monolayer on Cu(100). There exist two inequivalent molecular features; brighter protrusions (larger circle) and darker protrusions (smaller circle). The c(2 × 6) unit cell is also indicated. (c) 2D arrangement of the bottom part of the alkyl chains whose structure is optimized by force field calculations (see text). The 2D arrangement of the sulfur atoms and the methylene moieties that are directly bonded to the sulfur atoms is shown in the form of the projected view along the surface normal.

S−S1 distance was found to be 3.66 ± 0.05 Å, in accordance with the NN distance of the c(2 × 2) lattice (3.62 Å). Thus, these results indicate that the thiolates are initially distributed randomly over the surface occupying the 4-fold hollow sites, and afterward they form a 2D-ordered structure with a c(2 × 2)-S local arrangement.

IV. Discussion

A. Structural Model for the Saturated Phase. From the SEXAFS results, we propose a structural model for the 2D arrangement of the sulfur atoms as shown in Figure 12a. The LEED and XPS results indicate that this monolayer has a c(2 × 6) unit cell with a molecular density of 0.30 ± 0.03, from

which it is deduced that one unit cell contains 4 molecules. The sulfur atoms occupy the 4-fold hollow site with NN sulfur atoms at the same distance as for a c(2 × 2) lattice. The sulfur atoms are arranged into one-dimensional zigzag rows resulting in largely different distances to neighbor sulfur atoms (3.6 Å, 5.1 Å, 7.2 Å), while in bulk alkanes the alkyl chains pack into a quasi-hexagonal arrangement with similar chain−chain spacings along three major axes of the 2D-lattice (typically 4.2 Å, 4.5 Å, 5.0 Å).[44] The lattice mismatch between the sulfur layer and the alkyl layer is as much as 31% at maximum and would be usually unacceptable for epitaxial film growth due to too much strain. However, in the case of alkanethiol SAMs, the internal degrees of freedom play an important role to accommodate the strain.[9] To understand how the alkyl chains pack with the c(2 × 6)-S/Cu interface structure, we performed molecular mechanics calculations using a molecular simulation program, Cerius2 (MSI. Inc.). In the calculation, we assumed the periodic boundary condition for the commensurate c(2 × 6) unit cell with four S atoms fixed as shown in Figure 12a. A condensed-phase-optimized semiempirical force field (COMPASS)[45] was used in the calculation without including the Cu−S interaction. The alkyl-chain geometry was optimized from various trial structures and determined as the structure with the global minimum in total energy.

A bird's-eye view of the optimized structure is shown in Figure 13a. One-dimensional molecular rows are formed along the close-packed Cu rows. It should be noted that the molecular rows consist of two inequivalent rows; the C−C−C plane of half of the molecules is tilted from the surface normal and that of the other half almost vertical. Projected views seen from the direction along the molecular axes (Figure 13b) show that the molecules closely pack in a quasi-hexagonal arrangement with their carbon-backbone plane rotated around the molecular axes alternately by 90°, which is similar to the molecular packing seen for bulk alkanes.[43] The molecular axes are tilted by 32° on the average from the surface normal, which is consistent with the observed tilt angle (27 ± 5°) determined by C K-edge NEXAFS. Another interesting point of this structure is that there exist two types of S−C bond angle: one is almost vertical (5°), and the other is inclined (37°) as seen in Figure 13c.[46] The averaged S−C bond angle, i.e., 21°, is in agreement with the observed one (19 ± 10°) obtained from S K-edge NEXAFS. The tilting of half the S−C bonds allows the alkyl chains to pack into quasi-hexagonal arrangement with spacings of 4.1 Å, 5.1 Å, and 5.4 Å as is seen in the projected views shown in Figure 13b. This tilting effectively reduces the strain so that it decreases to 2%, 12%, and 7% for the three nearest neighbor spacings. Thus, the S−C bond layer acts as a buffer layer between the sulfur and the alkyl layers that have a large lattice mismatch.

B. Comparison of the Structural Model with a Molecular-Resolution STM Image. It is interesting to compare the above structure model with a molecular-resolution STM image shown in Figure 11b. The bright protrusions in the STM image also have the c(2 × 6) unit cell, but they show two types of brightness. The distance between the brighter protrusion and the adjacent darker one is 3.3 ± 0.3 Å, and they come into line along the unit vector of the primitive unit cell. On the other hand, in the model for the sulfur arrangement (Figure 12a), the second sulfur atom within the primitive unit cell is *not* situated on the unit vector. This discrepancy can be explained by the contribution of a density of state localized at the S−C bond to the STM molecular image.

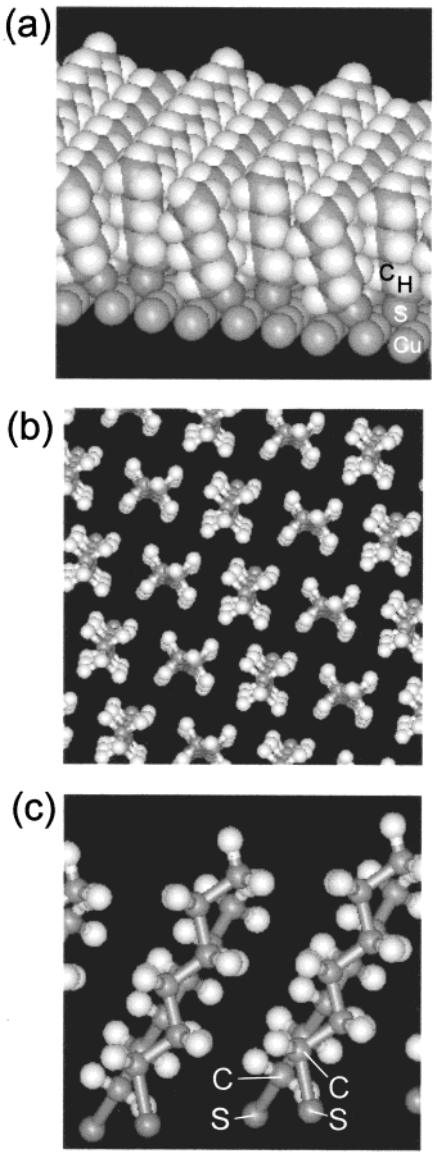

Figure 13. The geometry of the alkyl chains in the saturated monolayer on Cu(100) was optimized by the force field method assuming the fixed c(2 × 6)-S lattice (see text). (a) A bird's-eye view of the optimized structure. Two inequivalent molecular rows are formed along the close-packed Cu rows. (b) Projected views along the molecular axis. The alkyl chains pack into a quasi-hexagonal arrangement with the C−C−C plane being rotated by 90° alternately. (c) A side view along the next-nearest-neighbor direction. The C−C−C axes are tilted by 32° on the average, and the S−C bonds are titled in two ways: 5° and 37° from the surface normal.

Since the molecular image shown here was taken with a positive sample bias (V_B = +1.71 V), STM should visualize predominantly the lowest-unoccupied state of the adsorbed thiolate. According to the ab initio calculations for a methylthiolate adsorbed on noble metal surfaces,[40] the lowest-unoccupied state is the antibonding π-orbital with respect to the S−C bond (π^*(S−C)) whose electron density is most populated both on the S and the C atoms. In the present case, it is observed as a pre-edge small feature in the S K-edge NEXAFS spectra as shown in Figure 7. Thus, if the S−C bond is nearly normal, the protrusion coincides with the S position. If the S−C bond were tilted from the surface normal, however, the protrusion would be shifted from the S position. Figure 12c shows the 2D arrangement of the methylene moiety directly bonded to the sulfur atom, which reproduces the STM image well. The brighter

and darker protrusions in the STM image may be assigned to the two different local geometries of the S−C bonds (vertical and tilted orientations). Thus, the proposed structural model is reconciled with the molecular image if significant contribution of the π^*(S−C) orbital is taken into account. This interpretation is further supported by the presence of two domains, A and B, in the STM image as shown in Figure 3. These domains are rotated from the [011] direction and can be associated with the molecular axis tilting to opposite azimuthal directions. If the sulfur atoms were imaged in STM, only a single type of the c(2 × 6) domain should be observed.

C. Growth Process of the Alkanethiol SAMs on Cu(100). The change in molecular orientation during growth of the alkanethiol SAMs on Cu(100) is such that initially the molecules adsorb with lying-down configuration, start rising on the surface with increasing coverage, and finally stand up with a tilt angle of 27 ± 5° from the surface normal. Similar behavior has been observed for alkanethiol SAMs formed from solution on Au(111)[47] and from the gas phase under UHV conditions on Au(111),[3,14] Cu(111), and oxygen-covered Cu(111).[48] This kind of growth process might be rather general for alkanethiolate SAMs grown on metal substrates. However, the following three points are different from the growth process on Au(111) from the gas phase. (1) The sticking probability of the gaseous thiol onto Cu(100) is much higher than that onto Au(111). (2) The "striped phase" frequently observed on Au(111) at low coverages is absent on Cu(100). (3) It takes a much longer time for the saturated monolayer on Cu(100) to form the ordered structure after exposure.

To reach the saturated coverage of alkanethiol SAMs at room temperature, more than 5×10^5 L of exposure is necessary on Au(111),[14] while only 3 L dosing is enough on Cu(100). This can be explained by the fact that the Cu 3d band, which has a higher binding energy than Au 5d by 2 eV, contributes more significantly to dissociative chemisorption of the SH group, which results in more facile formation of the S−metal bond on the Cu substrate.

The striped phases have been found on Au(111) independent of alkyl-chain length and interpreted as 2D-ordered flat-lying phases where the stripes' period is in good agreement with the length of the corresponding fully stretched disulfide.[49] The thiolates in the striped phase are adsorbed with their C−C−C plane parallel to the surface and arranged in such a way that the intermolecular interactions are maximized as seen for self-assembly of *n*-alkanes on Au(111).[50] It seems essential for the formation of the striped phase that the S−C bond is inclined to the surface and the lateral diffusion of the thiolates is easy enough to reach a thermodynamically stable structure. Very recently, a combined study of the surface vibrational technique and the density functional theory calculations revealed that CH_3S adsorbed on Au(111) occupy the bridged site with the S−C bond tilted from the surface normal by 53°.[51] Thus, the largely inclined orientation of the S−C bond is reconciled with the flat configuration of the carbon-backbone plane. On the other hand, in the case of thiolates on Cu(100) the vertical orientation may be preferred as evidenced by the vertical S−C orientation found for CH_3S adsorbed on Cu(100).[24] This orientation preference prevents the carbon-backbone plane from lying parallel to the surface and induces the multi-configurations of the carbon-backbone plane resulting in nonunique intermolecular interactions. The important role of the orientation of the S−C bond to the SAM structures has been already pointed out on the Au and Ag surfaces.[52,53] Furthermore, the stronger S−Cu interactions significantly suppress the surface diffusion of the thiolates that is crucial to form a 2D-ordered structure.

The third difference (a much longer time is required for ordering on Cu(100)) is also related to the slow diffusion of the surface thiolates due to the stronger S−Cu interactions. In-situ STM observations of a hexanethiolate-saturated Cu(111) surface also indicated that it needs an aging time of 4 h after completion of the exposure to form an ordered structure,[54] while a hexanethiolate-saturated Au(111) surface exhibited ordered structures immediately after exposure.[14] It is noted that a large number of defects are observed in the c(2 × 6) structure even at thermal equilibrium as shown in Figure 2c, which also suggests insufficient surface diffusion of the thiolates on the Cu(100) surface.

The rate-limiting process for the SAM formation in the present system is not molecule−substrate bond formation or stretching of alkyl chains[55] but the 2D-ordering of the saturated monolayer. The surface thiolates in the saturated monolayer are initially distributed randomly over the 4-fold hollow sites even though the molecular axes are highly oriented. The absence of molecular features in the STM image of the saturated monolayer just after adsorption (Figure 1b,c) is explained by surface diffusion of the thiolates probably via hopping from one hollow site to another. After a prolonged time the thiolates are arranged into the 2D-ordered structure. The rate-limiting process is dominated by the strong S/Cu interaction.

V. Conclusions

The structure and growth process of hexanethiolate SAMs on Cu(100) have been studied by STM and XAFS. At low coverages surface thiolates are adsorbed with their molecular axis lying down to the surface. With increasing coverage the molecular axis gradually rises, and finally they form a standing-up monolayer with the molecular axis tilted by 27 ± 5° from the surface normal at saturated coverage. No 2D-ordered structure appears in the saturated monolayer just after adsorption. At this stage the surface thiolates randomly occupy 4-fold hollow sites and migrate probably via site exchange between the hollow sites. The saturated monolayer exhibits quite a slow evolution to a 2D-ordered phase with a c(2 × 6) periodicity, in which the sulfur atoms form 1D zigzag rows along the close-packed Cu rows. There is a significant lattice mismatch between the c(2 × 6)-S layer and the bulk-alkane layer. This mismatch is effectively reduced by tilting half the S−C bonds. The S−C layer plays an important role to reconcile the large lattice mismatch and form a SAM film on Cu(100).

Acknowledgment. The authors acknowledge Y. Kitajima of Photon Factory for his help with performing XAFS experiments. The authors are grateful for the financial support of the Ministry of Education, Sports and Culture (Grant 11640576). This research was performed under the approval of the Photon Factory Program Advisory Committee (PF-PAC 99G078). H. Kondoh acknowledges financial support from the Toyota Physical and Chemical Research Institute.

References and Notes

(1) Dubois, L. H.; Nuzzo, R. G. *Annu. Rev. Phys. Chem.* **1992**, *43*, 437.
(2) Ulman, A. *Chem. Rev.* **1996**, *96*, 1533.
(3) Poirier, G. E. *Chem. Rev.* **1997**, *97*, 1117.
(4) Fenter, P.; Eberhardt, A.; Eisenberger, P. *Science* **1994**, *266*, 1216.
(5) Fenter, P.; Schreiber, F.; Berman, L.; Scoles, G.; Eisenberger, P.; Bedzyk, M. J. *Surf. Sci.* **1998**, *412/413*, 213.
(6) Houssiau, L; Graupe, M.; Colorado, R., Jr.; Kim, H. I.; Lee, T. R.; Perry, S. S.; Rabalais, J. W. *J. Chem. Phys.* **1998**, *109*, 9134.

(7) Grönbeck, H.; Curioni, A.; Andreoni, W. *J. Am. Chem. Soc.* **1999**, *122*, 3839.

(8) Camillone, N., III; Chidsey, C. E. D.; Liu, G.; Scoles, G. *J. Chem. Phys.* **1993**, *98*, 3503.

(9) Fenter, P.; Eberhardt, A.; Liang, K. S.; Eisenberger, P. *J. Chem. Phys.* **1997**, *106*, 1600.

(10) Poirier, G. E.; Tarlov, M. J.; Rushmeier, H. E. *Langmuir* **1994**, *10*, 3383.

(11) Camillone, N., III; Leung, T. Y. B.; Schwartz, P.; Eisenberger, P.; Scoles, G. *Langmuir* **1996**, *12*, 2737.

(12) Himmel, H.-J.; Wöll, Ch.; Gerlach, R.; Polanski, G.; Rubahn, H.-G. *Langmuir* **1997**, *13*, 602.

(13) Balzer, F.; Gerlach, R.; Polanski, G.; Rubahn, H.-G. *Chem. Phys. Lett.* **1997**, *274*, 145.

(14) Kondoh, H.; Kodama, C.; Sumida, H.; Nozoye, H. *J. Chem. Phys.* **1999**, *111*, 1175.

(15) Fenter, P.; Eisenberger, P.; Li, J.; Camillone, N., III; Bernasek, S.; Scoles, G.; Ramanarayanan, T. A.; Liang, K. S. *Langmuir* **1991**, *7*, 2013.

(16) Heinz, R.; Rabe, J. P. *Langmuir* **1995**, *11*, 506.

(17) Dhirani, A.; Hines, M. A.; Fisher, A. J.; Ismail, O.; Guyot-Sionnest, P. *Langmuir* **1995**, *11*, 2609.

(18) Loepp, G.; Vollmer, S.; Witte, G.; Wöll, Ch. *Langmuir* **1999**, *15*, 3767.

(19) Driver, S. M.; Woodruff, D. P. *Langmuir* **2000**, *16*, 6693.

(20) Driver, S. M.; Woodruff, D. P. *Surf. Sci.* **2000**, *457*, 11.

(21) Himmelhaus, M.; Gauss, I.; Buck, M.; Eisert, F.; Wöll, Ch.; Grunze, M. *J. Electron. Spectrosc. Relat. Phenom.* **1998**, *92*, 139.

(22) Rieley, H.; Kendall, G. K. *Langmuir* **1999**, *15*, 8867.

(23) Prince, N. P.; Seymour, D. L.; Woodruff, D. P.; Jones, R. G.; Walter, W. *Surf. Sci.* **1989**, *215*, 566.

(24) Imanishi, A.; Takenaka, S.; Yokoyama, T.; Kitajima, Y.; Ohta, T. *J. Phys. (Paris)* **1997**, *IV7*−*C2*, 701.

(25) Hutt, D. A.; Cooper, E.; Leggett, G. J. *Surf. Sci.* **1998**, *397*, 154.

(26) Imanishi, A.; Isawa, K.; Matsui, F.; Tsuduki, T.; Yokoyama, T.; Kondoh, H.; Kitajima, Y.; Ohta, T. *Surf. Sci.* **1998**, *407*, 282.

(27) Tsuduki, T.; Imanishi, A.; Isawa, K.; Terada, S.; Matsui, F.; Kiguchi, M.; Yokoyama, T.; Ohta, T. *J. Synchrotron Rad.* **1999**, *6*, 787.

(28) Floriano, P. N.; Schlieben, O.; Doomes, E. D.; Klein, I.; Janssen, J.; Hormes, J.; Poliakoff, E. D.; McCarley, R. L. *Chem. Phys. Lett.* **2000**, *321*, 175.

(29) Kondoh, H.; Tsukabayashi, H.; Yokoyama, T.; Ohta, T. *Surf. Sci.* **2001**, *489*, 20.

(30) Jackson, G. J.; Woodruff, D. P.; Jones, R. G.; Singh, N. K.; Chan, A. S. Y.; Cowie, B. C. C.; Formoso, V. *Phys. Rev. Lett.* **2000**, *84*, 119.

(31) Namba, H.; Daimon, H.; Idei, Y.; Kosugi, N.; Kuroda, H.; Taniguchi, M.; Suga, S.; Murata, Y.; Ueyama, K.; Miyahara, T. *Rev. Sci. Instrum.* **1989**, *60*, 1909.

(32) Ohta, T.; Stefan, P. M.; Nomura, M.; Sekiyama, H. *Nucl. Instrum. Methods A* **1986**, *A246*, 373; Kitajima, Y. *J. Electron Spectrosc. Relat. Phenom.* **1996**, *80*, 405.

(33) Poirier, G. E. *J. Vac. Sci. Technol. B* **1996**, *14*, 1453.

(34) Vollmer, S.; Fouquet, P.; Witte, G.; Boas, Ch.; Kunat, M.; Burghaus, U.; Wöll, Ch. *Surf. Sci.* **2000**, *462*, 135.

(35) Stöhr, J. *NEXAFS Spectroscopy*; Springer: Heidelberg, 1992.

(36) Bagus, P. S.; Weiss, K.; Schertel, A.; Wöll, Ch.; Brunn, W.; Hellwig, C.; Jung, C. *Chem. Phys. Lett.* **1996**, *248*, 129.

(37) Väterlein, P.; Fink, R.; Umbach, E.; Wurth, W. *J. Chem. Phys.* **1998**, *108*, 3313.

(38) The orientation angle is deduced from polarization dependence of the intensity of the 1s → the σ^*(C−C) peak, which is estimated by curve-fitting with a step function and gauss functions as was performed in our previous works.[26, 27]

(39) Chauvistre, R.; Hormes, J.; Hartmann, E.; Etzenbach, N.; Hosch, R.; Hahn, J. *Chem. Phys.* **1997**, *223*, 293.

(40) Sellers, H.; Ulman, A.; Shnidman, Y.; Eilers, J. E. *J. Am. Chem. Soc.* **1993**, *115*, 9389.

(41) *X-ray Absorption: Principles, Applications, Techniques of EXAFS, SEXAFS and XANES*; Koningsberger, D. C., Prins, R., Eds.; Wiley: New York, 1988.

(42) Yokoyama, T.; Hamamatsu, H.; Ohta, T. Computer code EXAFSH, Version 2.1; The University of Tokyo, 1993.

(43) Ankudinov, A. L.; Ravel, B.; Rehr, J. J.; Conradson, S. D. *Phys. Rev. B* **1998**, *58*, 7565.

(44) Kitaigoroskii, A. K. *Organic Chemistry Crystallography*; Consultants Bureau: New York, 1961; Ungar, G. *J. Chem. Phys.* **1983**, *87*, 689; Sirota, E. B.; King, H. E., Jr.; Singer, D. M.; Shao, H. *ibid.* **1993**, *98*, 5809.

(45) The force field COMPASS has been developed by a hybrid approach consisting of ab initio and empirical method based on the ab initio force field CFF93 (M. J. Hwang, T. P. Stockfish, and A. T. Hagler, *J. Am. Chem. Soc.* **1994**, *116*, 2515). The most improved point for the COMPASS force field is that van der Waals parameters between nonbonding atoms were optimized using molecular dynamics (MD) simulations of condensed phase to reproduce the experimental data of cohesive energy and equilibrium density. By this force field the molecular structure and the crystal cell parameters of *n*-hexane were well reproduced within deviations of approximately 1% and 3%, respectively. H. Sun, *J. Phys. Chem. B* **1998**, *102*, 7338.

(46) In this geometry optimization, the molecule−substrate interactions are not taken into account. Therefore, the Cu(100) substrate plays a role of just a template for the c(2 × 6)-S structure in the calculation. Although the alkyl−copper interactions are negligible for the standing-up molecular orientation, potential for Cu−S−C angle obviously tends to force the S−C bond to stand up. Since this potential is not considered in the calculation, the resultant tilt angle (37°) should be considered as the maximum.

(47) Yamada, R.; Uosaki, K. *Langmuir* **1997**, *13*, 5218.

(48) Kondoh, H.; Ehara, Y.; Nambu, A.; Yokoyama, T.; Ohta, T. To be published.

(49) Camillone, N., III; Leung, T. Y. B.; Schwartz, P.; Eisenberger, P.; Scoles, G. *Langmuir* **1997**, *12*, 2737.

(50) Uosaki, K.; Yamada, R. *J. Am. Chem. Soc.* **1999**, *121*, 4090.

(51) Hayashi, T.; Morikawa, Y.; Nozoye, H. *J. Chem. Phys.* **2001**, *114*, 7615.

(52) Zharnikov, M.; Frey, S.; Rong, H.; Yang, Y.-J.; Heister, K.; Buck, M.; Grunze, M. *Phys. Chem. Chem. Phys.* **2000**, *2*, 3359.

(53) Rong, H.; Frey, S.; Yang, Y.-J.; Zharnikov, M.; Buck, M.; Wuhn, M.; Wöll, Ch.; Helmchen, G. *Langmuir* **2001**, *17*, 1582.

(54) Kondoh, H.; Saito, N.; Ohta, T. Unpublished.

(55) Hahner, G.; Wöll, Ch.; Buck, M.; Grunze, M. *Langmuir* **1993,** *9*, 1955.